

Demonstration of High-Efficiency Microwave Heating Producing Record Highly Charged Xenon Ion Beams with Superconducting ECR Ion Sources

X Wang^{1,2}, J B Li^{1,2}[‡], V Mironov³, J W Guo¹, X Z Zhang^{1,2},
O Tarvainen⁴, Y C Feng¹, L X Li¹, J D Ma¹, Z H Zhang¹,
W Lu^{1,2}, S Bogomolov³, L Sun^{1,2}[§], and H W Zhao^{1,2}

¹ Institute of Modern Physics, Chinese Academy of Sciences, Lanzhou 730000, People's Republic of China

² School of Nuclear Science and Technology, University of Chinese Academy of Sciences, Beijing 100049, People's Republic of China

³ Joint Institute for Nuclear Research, Flerov Laboratory of Nuclear Reactions, Dubna, Moscow Reg. 141980, Russia

⁴ UK Research and Innovation, STFC Rutherford Appleton Laboratory, Harwell Campus, OX11 0QX, United Kingdom

Abstract. Intense highly charged ion beam production is essential for high-power heavy ion accelerators. A novel movable Vlasov launcher for superconducting high charge state Electron Cyclotron Resonance (ECR) ion source has been devised that can affect the microwave power effectiveness by a factor of about 4 in terms of highly charged ion beam production. This approach based on a dedicated microwave launching system instead of the traditional coupling scheme has led to new insight on microwave-plasma interaction. With this new understanding, the world record highly charged xenon ion beam currents have been enhanced by up to a factor of 2, which could directly and significantly enhance the performance of heavy ion accelerators and provide many new research opportunities in nuclear physics, atomic physics and other disciplines.

Keywords: electron cyclotron resonance (ECR) ion source, magnetically confined plasma, microwave technology, highly charged ion beam

[‡] jiboli@impcas.ac.cn

[§] sunlt@impcas.ac.cn

1. Introduction

As the most powerful machine to produce intense highly charged ion beams, the Electron Cyclotron Resonance (ECR) ion source [1] has been invented for more than 50 years. It has played an indispensable role in accelerator based nuclear, atomic and material physics as well as various applications, such as exotic nuclei investigation, new elements synthesis, new material discoveries and heavy ion cancer treatment. To expand the nuclear landscape and probe properties of the nuclei in previously inaccessible regions of the nuclide chart, a significant number of next generation heavy ion accelerators are under construction [2, 3, 4, 5]. The increasing beam intensity need of these high-power heavy ion accelerators far exceeds the performance of state-of-the-art ECR ion source. For example, the international HIAF (High Intensity heavy ion Accelerator Facility) project requires the ECR ion source to deliver 0.7 emA of $^{238}\text{U}^{35+}$ beam in continuous wave (CW) mode, with the currently existing ion sources reaching only 0.35 emA [6]. In order to fulfill the requirements of advanced accelerators for intense highly charged heavy ion beams, the performance of ECR ion source must be improved considerably.

The ECR ion source is a device with a magnetically confined plasma sustained by microwave radiation. The electrons in the plasma are heated through electron cyclotron resonance heating (ECRH) to high energies by the electric field of the coupled microwave power, and the highly charged ions are produced by electron impact ionization while they are confined in the plasma up to hundreds of milliseconds. Thus, the performance of the ECR ion source is directly influenced by the efficiency of coupling the microwave energy to the plasma electrons. Tracing back to history, the development of ECR ion sources has always been accompanied by advancements in microwave coupling techniques. In general, for microwave frequencies $f \leq 18$ GHz, most ECR ion sources adopt a rectangular waveguide excited with a single TE_{10} mode [7]. This approach works well for microwave power levels up to 2 kW [8], corresponding to the maximum output power of an 18 GHz klystron amplifier. For microwave frequencies $f > 20$ GHz, a gyrotron is used to generate the microwave power up to 10 powers. Following the first successful injection of 28 GHz microwaves into the SERSE ion source [9], all subsequent 3rd generation ECR ion sources [10, 11, 12], which represent the state-of-the-art of high charge state ECR ion source technologies and performances, use an oversized circular waveguide ($\Phi = 32$ mm) to launch TE_{01} mode microwave radiation into the plasma. However, the coupling efficiency at frequencies above 20 GHz is questionable, since it has been verified experimentally [8] that at a fixed microwave power level of gyrotron frequencies, the ion source performance fails to follow the theoretical prediction by the ‘frequency scaling laws’ (beam intensity $I \propto f^2$) [1]. The less-than-expected microwave heating efficiency severely restricts performance of modern superconducting ECR ion sources and thus becomes an urgent issue for advanced heavy ion accelerators. Moreover, without remarkable progress, this conundrum would become a more severe problem for the next generation ECR ion source operating at an even higher frequency ($f > 40$ GHz) [6].

Over the past decade, continuous efforts have been put into improving the coupling

efficiency of the gyrotron frequency heating. Injection of the microwaves in the HE_{11} mode was firstly proposed [8] for better ECRH because of the Gaussian spatial profile of that particular EM-wave mode, but so far two experimental explorations have failed to demonstrate the expected improvements [13, 14]. Later on researchers at IMP (Institute of Modern Physics, Chinese Academy of Sciences) found that a circular waveguide with smaller diameter ($\Phi = 16 - 20$ mm) could improve the ion source performance at the same microwave power level. Qualitative interpretation of the observation is that the improved performance is due to the optimization of the power distribution on the ECR surface [15]. Because of the off-axis microwave injection structure in the ion source, this observation gives a hint that an asymmetric Vlasov launcher [16] would be more suitable to control the microwave power distribution on the ECR surface. Indeed, preliminary tests demonstrated that the beam current could be increased with a TE_{01} mode Vlasov launcher [15]. However, the position of the Vlasov launcher with respect to the plasma chamber was fixed in these experiments, it was not possible to systematically investigate or optimise the effect of the power distribution on the ECR surface.

To investigate further what the optimal way of injecting the microwaves with frequency above 20 GHz into the plasma in ECR ion source is, a novel movable Vlasov launcher has been developed at IMP. In this paper, we report the experimental and numerical researches on optimizing the microwave coupling of a superconducting ECR ion source with the new launcher.

2. Experimental Setup

The experimental data discussed hereafter are taken with the SECRAL-II (Superconducting ECR ion source with Advanced design in Lanzhou No. II) ion source, which is a superconducting ECR ion source developed at IMP. As a 3rd generation ECR machine, SECRAL-II exhibits high performance in the production of intense highly charged ion beams in CW mode with a number of beam intensity records, a schematic drawing of the ion source is shown in Figure 1 (a) and comprehensive description can be found in Ref. [6].

The schematic diagram of the movable Vlasov launcher is shown in Figure 1 (b). A standard circular waveguide (inner diameter $\Phi = 32$ mm) is connected to an 8 kW GyCOM[®] 24 GHz gyrotron with the other end of this waveguide connected to a smaller water-cooled circular waveguide (inner diameter $\Phi = 20$ mm) through a transition piece. Then a Vlasov launcher (refer to supplementary material, Section I) with an inner diameter of 23.6 mm is attached to the water-cooled waveguide ensuring good thermal and electrical contacts. The online movement of the Vlasov launcher is driven by a ball screw cylinder through a mechanical linkage without compromising the vacuum or having to turn off the microwave power or extraction voltage. The movable Vlasov launcher is inserted into the source chamber through an RF injection port at the SECRAL-II injection flange. The movable Vlasov launcher and relevant parts at the plasma chamber injection system are shown in Figure 1 (c).

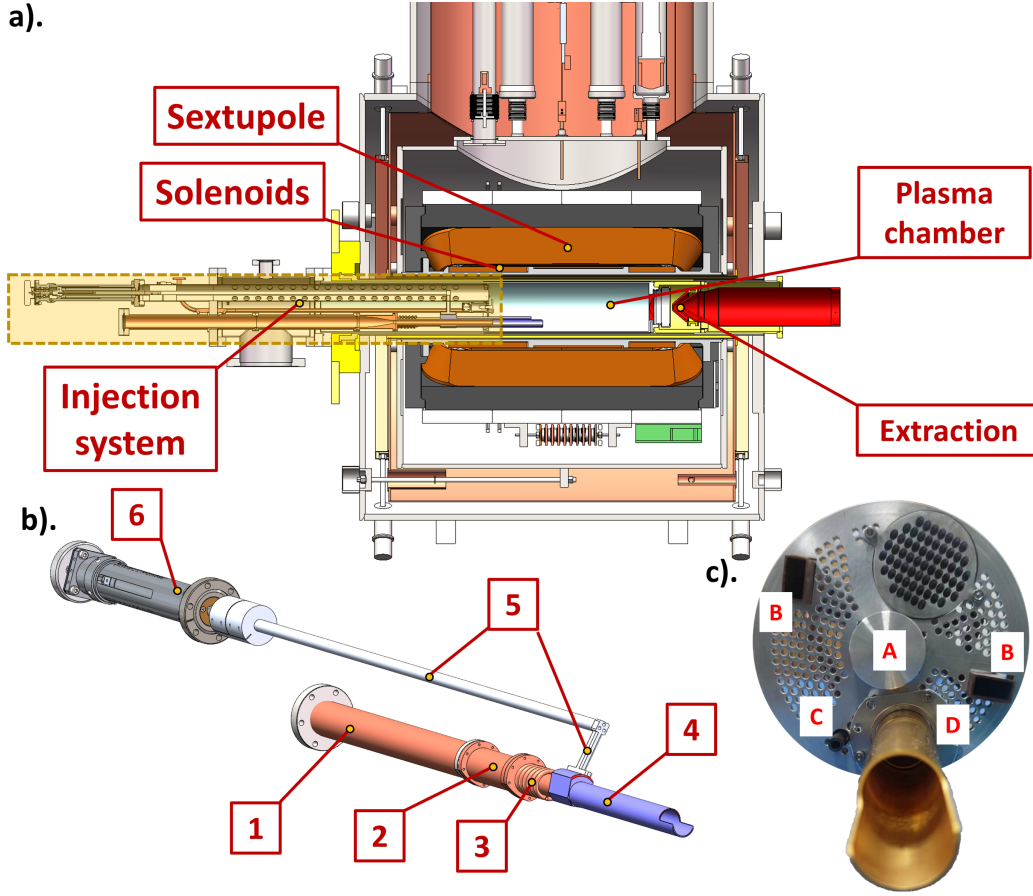


Figure 1. (a) The schematic drawing of the SECRAI-II ion source. (b) The schematic diagram of the movable Vlasov launcher, consisting of a standard circular waveguide (1), a 32 mm to 20 mm transition (2), a water-cooled circular waveguide (3), a Vlasov launcher (4), a mechanical linkage (5) and a ball screw cylinder (6). (c) Plasma chamber injection system of SECRAI-II ion source. The biased disc (A) is at the center, surrounded on both sides by two WR-62 type rectangular waveguides (B). The gas inlet (C) is at the bottom. The movable Vlasov launcher is located in place (D).

In this study, the position of the Vlasov launcher is varied from 0 mm, corresponding to an axial distance of 64 mm between the tip of the Vlasov launcher and the injection flange (the launcher cut length is of 30 mm), to 83 mm, the range being limited by the mechanical structure. Two-frequency heating is the standard option for the source operations since it suppresses kinetic instabilities [17] and enhances the temporal stability of the ion beams. Thus, one of the WR – 62 type rectangular waveguides is connected to an 18 GHz klystron amplifier as the supplemental heating. Both the WR–62 waveguide and the movable Vlasov launcher are equipped with vacuum windows and high voltage breaks. The source extraction voltage is 20 kV. In all measurements, the ion source is operated with xenon and oxygen buffer gas and tuned for high charge state xenon ion production, the main tuning parameters are magnetic field, gas pressure, and biased disk voltage. The ion beam currents are measured directly across a 1 k Ω

resistor connected to the Faraday cup located downstream from the beam analyzing magnet [18]. In addition, to investigate the influence of the Vlasov launcher position on the plasma electrons, the axial bremsstrahlung spectra in the energy range of 1 – 600 keV are synchronously measured. The detailed description of the bremsstrahlung detection system can be found in Ref. [19].

3. Experimental Results

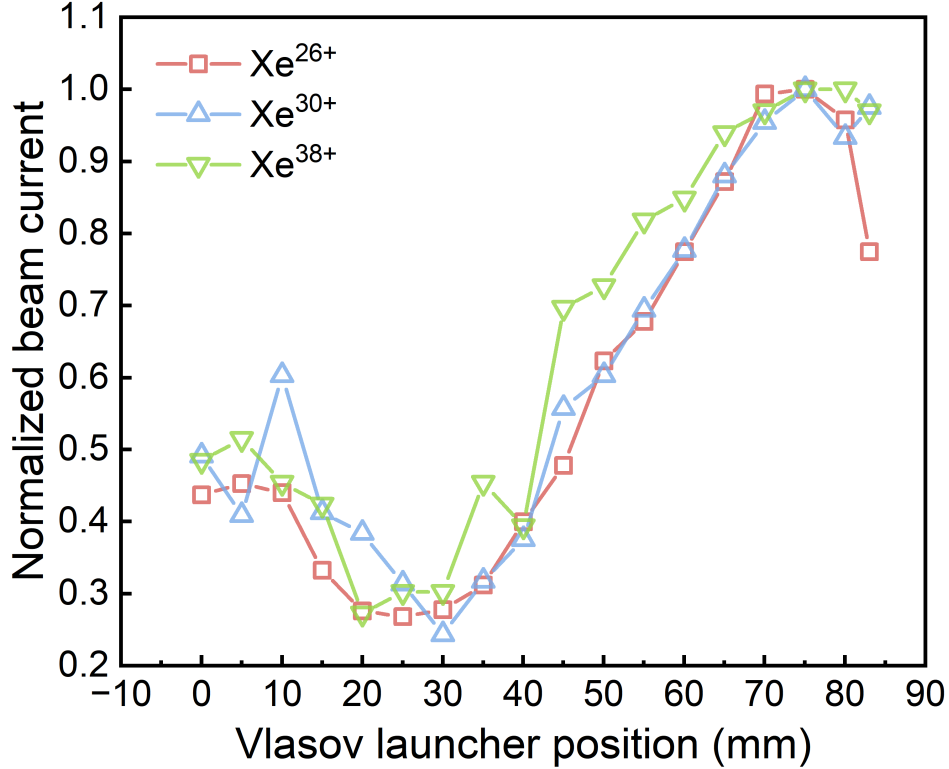


Figure 2. The normalized beam intensities of different charge state xenon beams as a function of the Vlasov launcher position. The microwave power of 24 GHz and 18 GHz are 4.5 and 0.5 kW, respectively. All beam currents in μA units are tabulated in the supplementary material, Table S1.

To investigate the effect of the Vlasov launcher position on the extracted beam currents, we first tune the ion source at the out-most position ($z = 0$ mm) to reach stable currents of the xenon ions with the specific charge state selected to measure. Then, the launcher position scan is done keeping all parameters constant. After the launcher is returned into initial position, the source is tuned for production of ions with another charge state and the procedure is repeated. Figure 2 presents the normalized beam intensities as a function of the Vlasov launcher position with different charge states, the values are normalized to their corresponding maxima. The microwave powers of 24 GHz and 18 GHz are fixed at 4.5 and 0.5 kW, respectively. It can be seen that the beam intensities initially decrease with the Vlasov launcher position until about 30 mm, and

then increase to their maximum values at 75 mm. A further increase of the position leads to a small drop in the beam currents. It should be noted that the distance between the optimum position ($z = 75$ mm) and the worst position ($z = 30$ mm) is 45 mm, which is much longer than the wavelength of the 24 GHz microwaves ($\lambda_{RF} = 12.5$ mm), thus suggesting that the observed behaviour is not due to standing wave formation. Meanwhile the beam currents obtained at the optimum position can be 4 times higher than in the worst case as shown in Table 1. Furthermore, the similar variation is also observed at different microwave power level (shown in the supplementary material Figure S2).

Table 1. The beam currents of different charge states at the best and the worst positions of the Vlasov launcher.

Ion	Beam current (Launcher at 75 mm)	Beam current (Launcher at 30 mm)
Xe ²⁶⁺	640 e μ A	178 e μ A
Xe ³⁰⁺	242 e μ A	59 e μ A
Xe ³⁸⁺	33 e μ A	10 e μ A

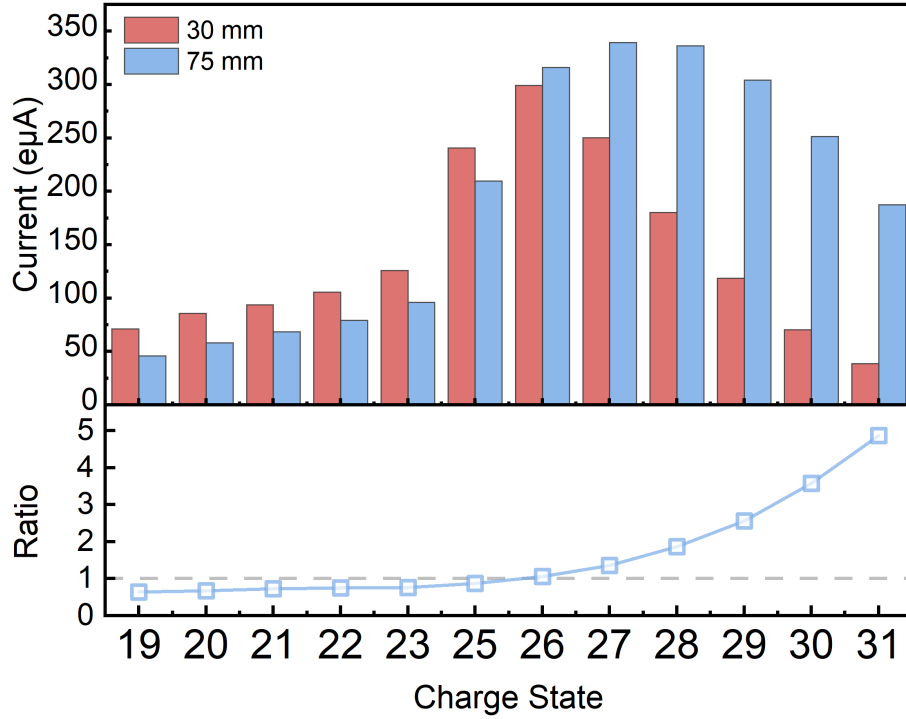


Figure 3. Xenon charge state distributions at the best and worst Vlasov launcher positions. Currents of Xe²⁴⁺ are not shown because they overlap with O³⁺. In addition, the gain factor of beam intensity at the best position compared to the worst position is presented.

The effect of the Vlasov launcher position on the xenon charge state distribution

(CSD) is also studied. The recorded m/q -spectra at the worst and best positions during the measurements of Xe^{30+} beam currents shown in Figure 2 are chosen for display in Figure 3, respectively. It is shown that the CSD peak is shifted to higher charge state (from Xe^{26+} to Xe^{27+}) when the Vlasov launcher is moved from the worst to the best position. The gain factor of beam intensity at the best position is greater than 1 for those ion beams with the charge states above the peak current CSD of the worst position, i.e., Xe^{26+} , and increases with the charge state, which indicates that optimization of the Vlasov launcher position is especially beneficial for the production of highly charged ions, similar to multiple frequency heating [20]. The total extracted ion current from the source (a leak current of the source HV power supply) reacts to the changes in the launcher position (see Figure 4) in parallel to the reaction of the highly charged ions. The current first decreases from 4.4 mA at the initial position down to 3.7 mA at the position 30 mm, and then increases up to 4.9 mA at 75 mm. As the total current is proportional to n_i/τ_i (ion density divided by the confinement time), the evolution of the total extracted ion current implies that either the plasma density is increased or the average confinement time of the ions is decreased at the optimum launcher position. The increase of the plasma density is considered more likely as the decrease of the confinement time should have an adverse effect on the very high charge state ion production.

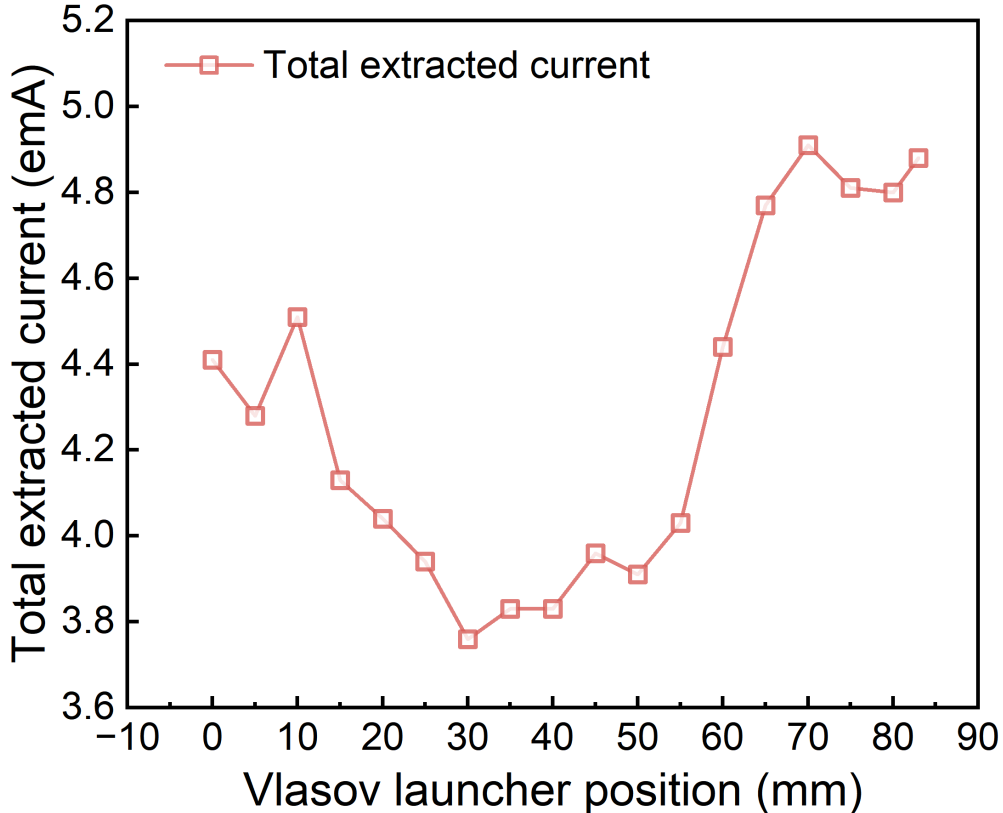


Figure 4. The total extracted current as a function of the Vlasov launcher position.

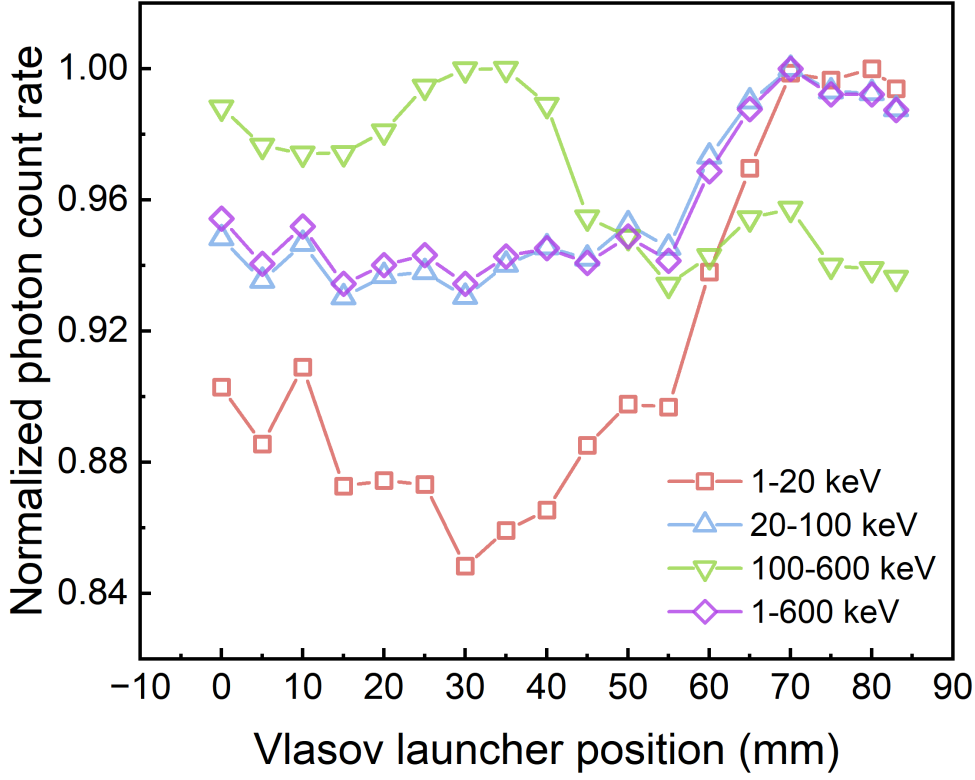


Figure 5. The normalized bremsstrahlung photon count rate within different energy intervals as a function of the Vlasov launcher position. The normalization is done to their corresponding maxima.

The influence of the Vlasov launcher position on the plasma electrons is studied indirectly by measuring the axial bremsstrahlung spectra. Figure 5 shows the normalized photon count rate within different energy intervals as a function of the Vlasov launcher position. The corresponding bremsstrahlung spectra are synchronously obtained during the measurements of Xe^{30+} beam currents shown in Figure 2 and corrected by the detector efficiency. We note that the measured bremsstrahlung spectrum is generated by collisions between electrons and neutrals or ions within the ECR plasma volume, plus electrons escaping the confinement colliding with the biased disk. Therefore, without deconvolution the bremsstrahlung spectra only indirectly reflect the electron energy distribution in the plasma and are affected by backward-scattered wall bremsstrahlung from the injection end of the ion source, i.e. flux of lost electrons. It is found that the total count rate is increasing by $\sim 7\%$ in the optimized launcher position. The bremsstrahlung count rate within the energy interval of $1 - 20$ keV is most affected by the launcher position, showing a tendency consistent with the beam current. For the photon count rate within the energy interval of $20 - 100$ keV, the variation tendency is similar to that of $1 - 20$ keV, but the relative change is much smaller. On the other hand, the photon count rate within the energy intervals of $100 - 600$ keV shows an almost opposite trend with that of $1 - 20$ keV, and reaches its maximum value at the worst position ($z = 30$ mm) implying that more high energy electrons are produced.

The original bremsstrahlung spectra at the best and worst position can be found from the supplementary material Figure S5, which supports the view of the launcher position affecting the plasma density. Moreover, the similar variation is also observed for Xe^{26+} and Xe^{38+} .

4. Numerical analysis

To better understand the experimental observations, we construct a full-size 3D model of the wave propagation and absorption in SECRAI-II ion source using the COMSOL Multiphysics[®] RF module [21]. In this model, the 3D cold-plasma conductivity tensor can be written as [22]:

$$\vec{\sigma} = \frac{\varepsilon_0 \omega_p^2}{i\omega + \nu} \frac{1}{1 + \beta^2} \begin{bmatrix} 1 + \beta_x^2 & \beta_x \beta_y + \beta_z & \beta_x \beta_z - \beta_y \\ \beta_y \beta_x - \beta_z & 1 + \beta_y^2 & \beta_y \beta_z + \beta_x \\ \beta_z \beta_x + \beta_y & \beta_z \beta_y - \beta_x & 1 + \beta_z^2 \end{bmatrix}. \quad (1)$$

In this expression,

$$\omega_p = \left(\frac{n_e e^2}{\varepsilon_0 m_e} \right)^{1/2} \quad (2)$$

is the electron plasma frequency,

$$\beta_k = \frac{\Omega_k}{i\omega + \nu} \quad (3)$$

is a dimensionless parameter with $k = x, y, z$,

$$\Omega_k = \frac{e B_k}{m_e} \quad (4)$$

is the electron cyclotron frequency with $k = x, y, z$, B_k is the magnitude of the magnetic field components in the $k = x, y, z$ directions, e and m_e are the electron charge and mass, respectively, n_e is the electron density in the plasma, ω is microwave frequency, and ν is the total collision frequency of electrons with ions and neutral atoms plus the effective collision frequency used as a free parameter. In our simulation, the microwave frequency and power are 24 GHz and 5 kW, the diameter and length of plasma chamber are 125 mm and 422 mm, respectively, and the 3D magnetic fields are calculated by the OPERA/Magnetostatic code using the coil current values used for tuning of Xe^{30+} in Figure 2. The electron density is set to $2.5 \times 10^{12} \text{ cm}^{-3}$ where magnetic field magnitude $B \leq 1.1 \times B_{\text{ecr}, 24\text{GHz}}$ (cold electron resonance field) and to 0 outside it. To avoid the solver's divergence, we set $\nu/\omega = 0.001$, similar to Ref. [23]. Although this approximation greatly simplifies the wave dynamics in the plasma, it enables us to estimate the basic features of the wave propagation and absorption. The 3D wave equations are solved by using an unstructured mesh with approximately 638,000 mesh points, resulting in a 5 mm spatial resolution for computational domains, small compared to the wavelength of 24 GHz microwave (12.5 mm). These simulations are performed on a in-house 64-bit Linux cluster using the PARADISO direct linear system solver in COMSOL Multiphysics[®].

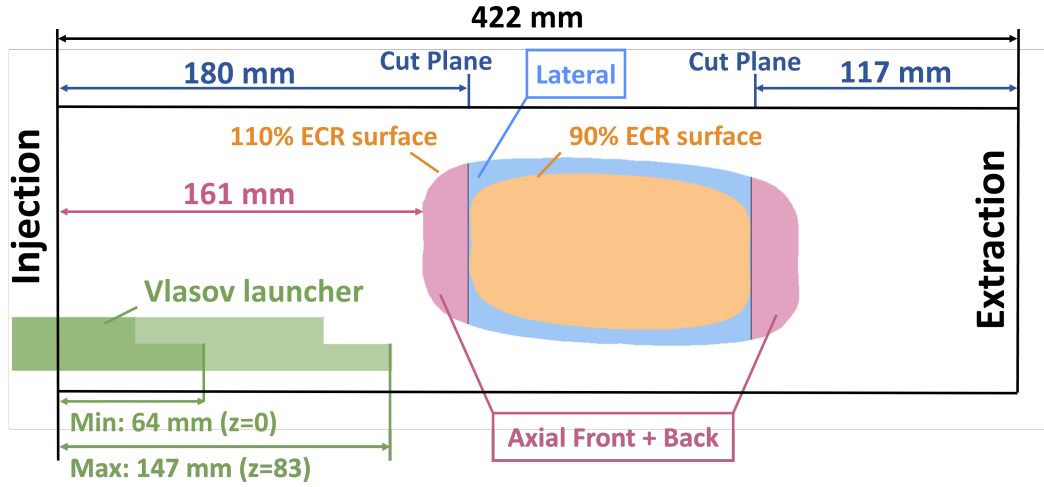


Figure 6. Computational domain and regions of interest in the COMSOL model.

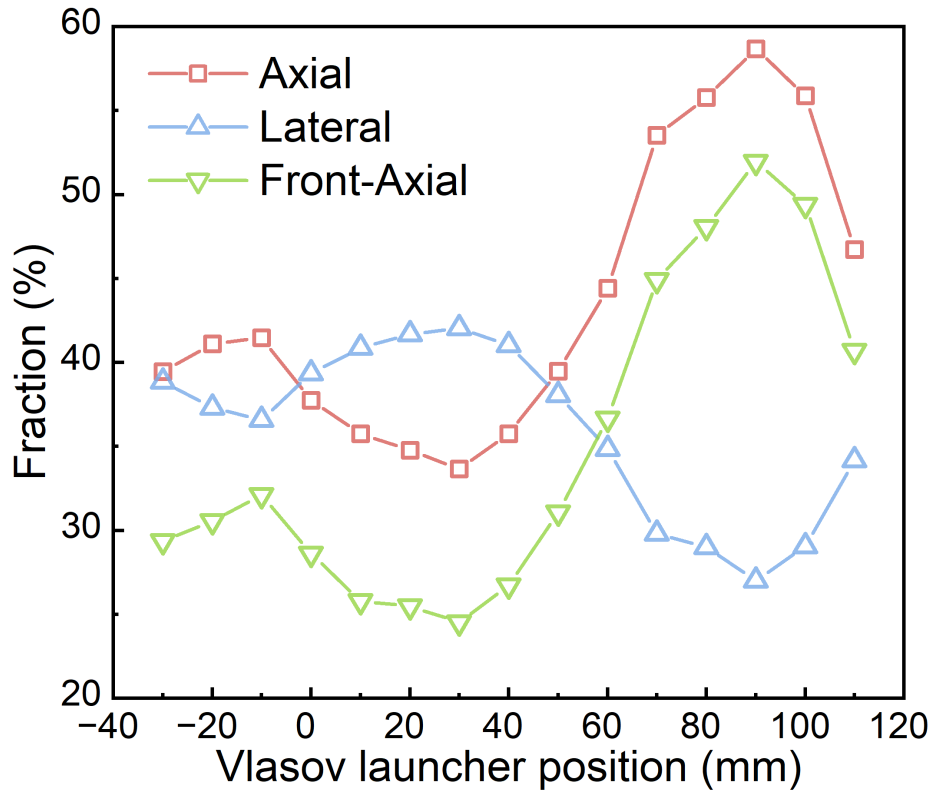


Figure 7. The fractional evolution in absorbed power with Vlasov Launcher position for axial, lateral and front-axial volumes.

The experimental observations (such as the emittance measurements of the extracted ion beams [24]), and the numerical simulations [25] indicate that the plasma in ECR ion sources is mostly localized close to the source axis inside the ECR zone. Since the wave propagation and absorption are strongly influenced by plasma density

close to the ECR surface [23, 26], such localization affects the microwave coupling efficiency. To spatially characterize the microwave absorption process, we divide our computational domain into several regions of interest: the region close to the cold electron resonance surface of 24 GHz frequency (in the plasma volume where $0.9 \times B_{\text{ecr},24\text{GHz}} \leq B \leq 1.1 \times B_{\text{ecr},24\text{GHz}}$), and the inner/outer parts for the rest of the domain. The ECR volume is additionally divided by two cutting planes into the axial-front, axial-back and the lateral parts as illustrated in Figure 6. The axial volume corresponds to the region where the core plasma [27] is supposed to be heated, while the lateral absorption is believed to be responsible for the halo plasma heating. The fractional evolution in absorbed power with Vlasov launcher position for axial (front + back), lateral and front-axial volumes are calculated (see Figure 7). According to the simulation model, the position of the Vlasov launcher affects significantly the absorbed power in the axial volume, especially in the front-axial volume. The dependency of the absorbed power in the front-axial volume with the launcher position exhibits good consistency with the experimental data of Xe^{30+} beam intensity (see Figure 2), the ratio of the maximum value to the minimum one is about 2. On the other hand, the absorbed power in the lateral volume shows an exactly opposite trend with that of front-axial volume, and reaches its maximum value at the worst position ($z = 30$ mm), which coincides with the worst high charge state ion production.

5. Discussion

Experiments on the microwave coupling scheme with some 2nd generation ECR ion sources [28, 29, 30] have demonstrated that the extracted beam currents are affected by the variations of microwave frequency (frequency tuning) and cavity dimensions (cavity tuning), and it has been argued [31] that the beam intensity variations are caused by the excitation of electromagnetic eigenmodes of the plasma chamber, which acts as a resonator cavity, and subsequent differences between the electron heating properties that presumably influence the plasma confinement and ionization rate, as well as ion dynamics. For a 3rd generation ECR ion source operating with much larger plasma chamber (an inner diameter of 125 mm for SECRAL-II) and higher frequency (i.e., a shorter wavelength of 12.5 mm for 24 GHz), the plasma chamber will act as an overmoded cavity in which the eigenmodes overlap due to plasma induced broadening. Then it can be expected [30] that the frequency tuning and cavity tuning effects would be less effective. Indeed, we do not see in the reported measurements any changes in the source behavior that can be attributed to the cavity tuning with the expected oscillations when moving the launcher by around $\lambda_{\text{RF}}/2$.

Strong gain in the source performance is observed when the Vlasov launcher is positioned such that the injected microwaves are focused on the ECR surface close the source axis – currents of the highly charged xenon ions vary by a factor of about 4 and more ions with higher charge state are produced at the optimized position. This suggests that the microwave launching scheme plays an important role in the production

of highly charged ion beams with superconducting ECR ion sources.

The recent numerical simulations [27, 32] demonstrated that the ECRIS plasma can be characterized as a combination of the cold dense core and the hot dilute halo plasmas. The reason for formation of these components is the different confinement dynamics for the electrons that reside close to the source axis and for those found at the peripheral parts of the magnetic trap. Close to the axis, the electron movement is governed by the solenoidal component of the source's magnetic field. The axial electrons stay confined close to the axis during their bouncing along the magnetic field lines, and their confinement is affected by electric fields close to the biased disk and the extraction aperture. The halo electron movement is more defined by the hexapole field component; curvature drifts of the axial and halo electrons have the opposite directions. The halo electrons cross the ECR surface more frequently and are supposed to be heated faster than the axial ones. The extracted ion currents are mostly defined by the core electron component, while the ion fluxes to the radial walls of the source are mostly produced in the halo plasma. From the point of view of the microwave coupling efficiency, it is preferable to heat the core plasma as much as possible and to reduce the power that is available for absorption by the halo electrons.

According to our simulations, the axial volume corresponds to the region where the core plasma is supposed to be heated, we see that the variation of the absorbed power in the front-axial volume is strong and shows a good consistency with the extracted currents of high charge state ions, while the absorbed power in the lateral volume, which is believed to be responsible for the halo plasma heating, shows an opposite trend with the beam currents. We argue that at least for a 3rd generation ECR ion source operating at frequency above 20 GHz, the location where the microwave power is absorbed is important for production of the highly charged ions, and the optimum microwave absorption region is close to the source axis. The improved microwave heating efficiency could be achieved by the optimization of the microwave launching scheme, i.e., directing the microwaves to the ECR surface close to the source axis as much as possible, so that more plasma electrons located in the dense core regions of the plasma can be effectively heated to the energies that are optimal for the highly charged ion production, i.e. electron impact ionization and electrostatic confinement in a potential dip formed by the confined electrons. This argument is supported by the diagnostic result: the evolution of the bremsstrahlung count rate in the energy interval of 100 – 600 keV indicates that more high energy (> 100 keV) electrons are produced at the worst position. As these high-energy electrons can also contribute to the photon count rate within the energy intervals of 1 – 20 keV, however, it is shown that the bremsstrahlung count rate in the energy interval of 1 – 20 keV is mostly affected by the Vlasov launcher movement and reaches a maximum at the best position. This should be due to more warm (1 – 20 keV) core electrons, which contribute part of the photon count rates within the energy intervals of 1 – 20 keV, and less high-energy electrons produced at the best position of the launcher. As a result, the spectral temperature T_s , which can be considered as an indication of the average electron energy [33, 34], reaches

its minimum value at the best position, the evolution of T_s with the Vlasov launcher position is presented in detail in the supplementary material Figure S6. Since these warm electrons are especially beneficial for the production of highly charged ions [35], the performance of the ion source is thus improved. Moreover, the diagnostic results also show that the Vlasov launcher position has only a weak effect on the photon counts within the energy interval of 100 – 600 keV, which suggests that position of the Vlasov launcher changes the shape of the electron energy distribution function (EEDF). This technique may be helpful for the suppression of kinetic instabilities [36] in ECR ion source plasma, which are driven by the anisotropy of the EEDF [37].

Table 2. The optimized xenon beam intensity results using the movable Vlasov launcher

Ion	Microwave power	Beam intensity	Records	Improvement
Xe ⁴²⁺	7 + 0.5 kW	18 eμA	12 eμA*	50 %
Xe ³⁸⁺	7.5 + 1 kW	47 eμA	23 eμA*	104 %
Xe ³⁴⁺	7.5 + 1 kW	146 eμA	120 eμA*	22 %

Condition: 24 + 18 GHz, 7 ~ 8 kW, movable Vlasov launcher.

*Traditional smaller circular waveguide ($\Phi = 16 - 20$ mm), 24 + 18 GHz, 7 ~ 8 kW. [15, 18]

Based on these arguments, we completed a preliminary optimization of highly charged xenon ion beams at high microwave power. The main tuning parameters are Vlasov launcher position, magnetic field, gas pressure, and biased disk voltage. It is encouraging to see from Table 2 that intense highly charged xenon ion beams (e.g., 146 eμA of Xe³⁴⁺) could be obtained by using the movable Vlasov launcher. The improvement, compared with the beam intensity records of SECRAL ion source using smaller circular waveguide, is up to a factor of 2 (for Xe³⁸⁺) at the same power level. Meanwhile, the online test at high frequency and high microwave power has proved that the movable Vlasov launcher is reliable and could be an option for the routine operation.

6. Summary

In summary, the present work experimentally and numerically demonstrates that for a 3rd generation ECR ion source operating at frequency above 20 GHz, the microwave heating efficiency is significantly affected by the microwave launching scheme and high-efficiency microwave heating could be achieved by using the movable Vlasov launcher technique. The remarkable improvement of highly charged ion beam intensity based on this novel technique could significantly boost the performance of the state-of-the-art machines in operation, which provides new possibilities to the physics goals as well as heavy ion accelerator facility performance, such as the 400 kW goal with FRIB accelerator [38], and the 10–20 pμA ⁵⁴Cr¹⁴⁺ beam for 119, 120 elements synthesis [39]. Meanwhile, this study points out a direction for further study and optimization of

microwave heating efficiency in modern superconducting ECR ion sources and thus gives a new insight into the design of microwave injection system for the next generation ECR ion sources. Nevertheless, the systematic parameter optimization, such as the launcher structure and the microwave mode, will be a topic of future investigations with state-of-the-art ECR ion sources.

7. Acknowledgments

The authors thank L. Celona and S. Gammino of INFN for helpful discussion, and D. Hitz for guidance on experimental design. This work has been supported by the National Natural Science Foundation of China (Grant Nos. 12025506, 11427904, and 12175285), the Key Scientific Instruments Development Program of CAS (Grant No. GJJSTD20210007), and the Natural Science Foundation of Gansu Province, China (Grant No. 23JRR A584).

8. References

- [1] Geller R 1996 *Electron Cyclotron Resonance Ion Sources and ECR Plasmas* (Routledge)
- [2] Zhou X, Yang J *et al.* 2022 *AAPPS Bulletin* **32** 35
- [3] Wei J, Ao H, Beher S *et al.* 2019 *Int J Mod Phys E* **28** 1930003
- [4] Delahaye H F 2022 The New GANIL Beams: Commissioning of SPIRAL 2 Accelerator and Resent Developments *Proc. HIAT'22* pp 124–129
- [5] Okuno H, Dantsuka T, Fujimaki M *et al.* 2020 *J. Phys.: Conf. Ser.* **1401** 012005
- [6] Zhao H, Sun L, Guo J *et al.* 2018 *Rev. Sci. Instrum* **89** 052301
- [7] Celona L, Gammino S, Ciavola G *et al.* 2010 *Rev. Sci. Instrum* **81** 02A333
- [8] Hitz D 2006 *Adv Imag Elect Phys* **144** 1–164
- [9] Gammino S, Ciavola G, Celona L *et al.* 2001 *AIP Conf Proc* **600** 223–227
- [10] Marks M, Evans S, Jory H *et al.* 2005 *AIP Conf Proc* **749** 207–210
- [11] Sun L, Lu W, Feng Y *et al.* 2013 *Rev. Sci. Instrum* **85** 02A942
- [12] Nakagawa T, Higurashi Y, Ohnishi J *et al.* 2010 *Rev. Sci. Instrum* **81** 02A320
- [13] Lyneis C, Benitez J, Hodgkinson A *et al.* 2013 *Rev. Sci. Instrum* **85** 02A932
- [14] Sun L, Guo J, Lu W *et al.* 2015 *Rev. Sci. Instrum* **87** 02A707
- [15] Guo J, Sun L, Lu W *et al.* 2020 *Rev. Sci. Instrum* **91** 013322
- [16] Vlasov S and Orlova I 1974 *Radiophys. Quantum Electron.* **17** 115–119
- [17] Skalyga V, Izotov I, Kalvas T *et al.* 2015 *Phys. Plasmas* **22** 083509 ISSN 1070-664X
- [18] Li L, Li J, Ma J *et al.* 2022 *Phys. Rev. Accel. Beams* **25** 063402
- [19] Li J, Li L, Bhaskar B S *et al.* 2020 *Plasma Phys. Control. Fusion* **62** 095015
- [20] Vondrasek R 2022 *Rev. Sci. Instrum* **93** 031501
- [21] 2022 *COMSOL Multiphysics® RF module*
- [22] van Ameijde D A 2021 *Microwave absorption in an ECR plasma: A theoretical analysis and computational implementation for unstructured meshes using vector finite elements* Master's thesis Eindhoven University of Technology
- [23] Cluggish B P and Kim J S 2012 *Nucl. Instrum. Methods. Phys. Res. A* **664** 84–97
- [24] Leitner D, Lyneis C, Abbott S *et al.* 2005 *Nucl Instrum Methods Phys Res B* **235** 486–493
- [25] Mironov V, Bogomolov S, Bondarchenko A *et al.* 2020 *Plasma Sources Sci Technol* **29** 065010
- [26] Mascali D, Torrisi G, Neri L *et al.* 2015 *Eur. Phys. J. D* **69** 27
- [27] Mironov V, Bogomolov S, Bondarchenko A *et al.* 2022 *J. Instrum* **17** P06028
- [28] Celona L, Ciavola G, Consoli F *et al.* 2008 *Rev. Sci. Instrum* **79** 023305

- [29] Maimone F, Celona L, Lang R *et al.* 2011 *Rev. Sci. Instrum* **82** 123302
- [30] Tarvainen O, Orpana J, Kronholm R *et al.* 2016 *Rev. Sci. Instrum* **87** 093301
- [31] Consoli F, Celona L, Ciavola G *et al.* 2008 *Rev. Sci. Instrum* **79** 02A308
- [32] Mironov V, Bogomolov S, Bondarchenko A *et al.* 2021 *J. Instrum* **16** P04009
- [33] Lamoureux M 2000 *Radiat. Phys. Chem* **59** 171–180
- [34] Kasthurirangan S, Agnihotri A N, Desai C A *et al.* 2012 *Rev. Sci. Instrum* **83** 073111
- [35] Benitez J, Lyneis C, Phair L *et al.* 2017 *IEEE Trans Plasma Sci* **45** 1746–1754
- [36] Tarvainen O, Izotov I, Mansfeld D *et al.* 2014 *Plasma Sources Sci. Technol.* **23** 025020
- [37] Shalashov A G, Gospodchikov E D, Izotov I V *et al.* 2018 *Phys. Rev. Lett.* **120**(15) 155001
- [38] Ostroumov P N, Fukushima K, Maruta T *et al.* 2021 *Phys. Rev. Lett.* **126**(11) 114801
- [39] Khuyagbaatar J, Yakushev A, Düllmann C E *et al.* 2020 *Phys. Rev. C* **102**(6) 064602